WATER RESOURCES RESEARCH, VOL. 37, NO. 5, PAGES 1425–1435, MAY 2001

A study of solute transport mechanisms using rare earth element tracers and artificial rainstorms on snow

Xiahong Feng,[1] James W. Kirchner,[2] Carl E. Renshaw,[1] Randall S. Osterhuber,[3] Björn Klaue,[4] and Susan Taylor[1,5]

Abstract. Rare earth element (REE) tracers and three artificial rain-on-snow storms at the Central Sierra Snow Laboratory, California indicate that (1) tracers applied to the snow surface immediately prior to the storm quickly appear at the bottom of the pack, with the tracer traversing the pack faster when the snowpack is wetter; (2) unlike most previous studies in which low solute concentrations were observed at high flow in diurnal cycles, the concentrations of the REE tracers in the outflow are positively related with input water flux; and (3) at a constant input flux the concentrations of all the REE tracers decreased exponentially with time, and the rate of this decrease was greater at high flow than at low flow. These observations can be qualitatively simulated by partitioning liquid water in the snowpack into mobile and immobile phases. Transport of the mobile water phase is governed by the advection-dispersion equations, while the immobile water only moves by exchanging with the mobile water. The rate of exchange between mobile and immobile waters follows first-order kinetics. Unlike previous mobile-immobile models for snow, the exchange rate coefficient is assumed to increase exponentially with the effective water saturation. The model successfully simulates the positive concentration dependency on input water flux. However, it remains unclear how the exchange rate coefficient varies with the nature of the medium and with hydrological conditions. These observations suggest that tracer concentrations in the outflow are largely dominated by solute transport via fast flow channels. This surprising result implies that a spatially averaged flow rate may not be adequate for modeling solute transport properties in unsaturated media.

1. Introduction

In temperate regions, snowmelt often accounts for the majority of the annual water input to a catchment and often causes the largest annual stream discharge event. Snowpacks accumulate and store atmospherically deposited chemical contaminants throughout the winter, and thus snowmelt often accounts for a large fraction of annual atmospherically derived solute inputs to the watershed. The chemical composition of meltwater generated from a snowpack does not equal the average composition in the snowpack itself but instead varies temporally as melting proceeds. Chemical impurities (such as SO_4^{2-}, NO_3^-, H^+, Na^+, K^+, Ca^{2+}, etc.) tend to be preferentially eluted from a snowpack during the earlier phases of snowmelt [*Bales et al*., 1989; *Colbeck*, 1981; *Johannessen and Henriksen*, 1978], in what is termed an ionic pulse. Ionic pulses are thought to be a major cause of stream and lake acidification during the spring runoff [*Cadle et al*., 1987; *Dickson*, 1980; *Galloway et al*., 1987; *Skartveit and Gjessing*, 1979]. Ionic pulses occur because solutes are segregated to the exterior of the snow grains or the pore fluid during snow metamorphism [*Bales et al*., 1993; *Colbeck*, 1981; *Cragin et al*., 1996; *Davis*, 1991; *Tsiouris et al*., 1985].

The magnitude of the ionic pulse for a given mature snowpack is dependent upon the solute transport mechanism. Two bounding end-member mechanisms are piston flow and preferential flow. In piston flow, water flows out in the sequence that it enters the medium and it carries all solutes down the hydraulic head gradient [*Hibberd*, 1984]. In preferential flow, only solutes in flow channels are effectively transported and those in the surrounding matrix are transported only after they enter a flow channel (e.g., by diffusion) [*Harrington and Bales*, 1998]. Certain observations can help distinguish these two flow end-members. With preferential flow, solute concentrations may decrease with increasing discharge, because high water flux dilutes the solute flux entering the flow channels. Piston flow may lack this concentration-discharge relationship. Instead, changes in solute concentration may lag discharge changes because of the kinematics of wave propagation. Which mechanism dominates a given flow system is a complicated problem which depends on both the intrinsic characteristics of the medium and its water content.

In this contribution, we describe a study of solute transport mechanisms in snow using a series of artificial rain-on-snow experiments at the Central Sierra Snow Laboratory (CSSL), California. Rare earth elements, sprayed onto the snowpack surface at intervals throughout the winter and immediately before each artificial rainstorm, were used as chemical tracers. The simple experimental setting and well-controlled experimental conditions allow us to distinguish among solute trans-

[1]Department of Earth Sciences, Dartmouth College, Hanover, New Hampshire.
[2]Department of Geology and Geophysics, University of California, Berkeley, California.
[3]Central Sierra Snow Laboratory, Soda Springs, California.
[4]Department of Geological Sciences, University of Michigan, Ann Arbor, Michigan.
[5]Also at U.S. Army Cold Regions Research and Engineering Laboratory, Hanover, New Hampshire.

Paper number 2000WR900376.
0043-1397/01/2000WR900376$09.00

port mechanisms and parameterize transport models, which may have implications for solute transport processes at watershed scales.

2. Site Information and Experimental Methods

The Central Sierra Snow Laboratory is located on the southwest crest of the Sierra Nevada near Soda Springs, California (39°22′19″N and 122°22′15″W), at an altitude of 2100 m. The snow laboratory is constructed in a 0.5 ha clearing in a pine forest. It is instrumented to measure meteorological variables including air temperature, precipitation, wind speed, humidity, and incident and reflected radiation (both long and short waves). Two large 6×3 m^2 melt pans, the north pan and south pan, collect water draining from the overlying snowpack. The bottom of the melt pan is sloped by 1.3% toward a corner, where meltwater drains, and the snow surface was visibly flat at the time of the experiment. Meltwater reaching the melt pan at the base of the pack flows to a corner, where it travels along an 8 m PVC pipe to a hut. Here the volume of runoff was measured and timed using a 4 L tipping bucket attached to a data logger.

The site receives about 80% of its precipitation in the form of snow. On average, the maximum accumulation in annual snowpacks at CSSL is ~90 cm of water equivalent. The rain-on-snow experiments reported in this paper were conducted in the spring of 1998. The maximum accumulation of that winter was 360 cm depth (~150 cm water equivalent). By the time the experiments began on June 9 the snowpack was fully ripe and had melted down to 135 cm. The pack was 120 cm thick at the end of the experiments on June 10. During the time of the experiments, the air temperature never fell below zero. The pack was measured to be isothermal in April, and we expect that it was also isothermal during our experiments. The bulk density measured in April was 0.42 ± 0.044 g cm^{-3} ($n = 134$), and we assume that this bulk density did not change significantly between April and June. Although this assumption may not be valid, it does not affect the conclusions of this work. The mean bulk density corresponds to a porosity of ~0.57, assuming the liquid water content of the snowpack (S_i) at the time of the measurement was 5% of the pore volume.

We generated three artificial rain-on-snow events above the north pan using lawn sprinklers and tap water. To monitor the amount and distribution of the rain, we used 18 plastic cups, one placed directly on each square meter of the snow surface overlying the north pan, to collect the precipitation. At the end of each storm the water in each cup was weighed and converted into millimeters of precipitation. To allow complete coverage of the north pan, the spray area is greater than the area of the pan by at least 2 m on each side of the pan. The first storm was produced in the morning of June 9. It was a cold morning with an air temperature of about 1°C, and the discharge was low (0.4 mm h^{-1}). The storm lasted 2.5 hours and the amount of precipitation was 32.6 ± 6.3 mm ($\pm 1\sigma$, among the 18 rain gauges). Storms 2 and 3 were both produced the following day, one in the predawn hours and the other in the afternoon. When storm 2 began, at about 3:00 A.M. PST, the snowpack was still draining water stored in the pack during the previous day, and the flow rate was 3.4 mm h^{-1}. This storm lasted 1.5 hours and had total 37.5 ± 7.9 mm of precipitation. At the onset of storm 3 the snowpack was even wetter than storm 2, having a flow rate of 5.8 mm h^{-1}. This storm lasted 4.5 hours and had total 95.5 ± 7.2 mm of precipitation. Between the second and the third artificial storms, there was ~5 mm of natural rain. The tap water temperature was 1°C. The total 165.6 mm of this tap water would cause the snow to melt by <5 mm. We consider this to be insignificant.

We used thulium (Tm), ytterbium (Yb), and lutetium (Lu) chlorides as chemical tracers, spraying them onto the snowpack surface immediately before each of the three artificial rainstorms and measuring their concentrations in meltwater from the bottom of the snowpack. As part of a related study [*Taylor et al*., 2001], we had also sprayed other rare earth element tracers on the snowpack surface as the snowpack accumulated during the winter in order to mark individual snow layers. Several tagged snow layers near the bottom of the snowpack, including those marked by praseodymium (Pr) and cerium (Ce), were still beneath the snow surface at the time of our artificial rainstorms, so those tracers presumably reflect the behavior of snow in situ within the melting pack. Snow layers higher in the snowpack, including those marked by europium (Eu), gadolinium (Gd), terbium (Tb), and holmium (Ho), had already been melted, so those tracers reflect the behavior of meltwaters that have been percolating through the remaining snowpack for days or weeks. One layer, marked by samarium (Sm), was exhumed and melted during our three artificial rainstorms.

Under typical snow conditions the rare earth element (REE) chlorides are all readily soluble at the concentrations used for the experiments (<25 ppm). Carbonate precipitation ultimately limits the solubility of the REE chlorides, but we calculate that even under the worst-case conditions expected for natural snow, REE carbonate precipitation should not occur. This calculation is based on equilibrium constants given by *Lee and Byrne* [1992, 1993] and the highest major ion concentrations recorded from 1989 to 1993 at CSSL. Prior to each of the rain events we sampled the discharge from the tipping bucket of the north pan and then sprayed a rare earth element tracer solution onto the snow surface using a compressed air sprayer. Tm, Yb, and Lu chlorides were sequentially used for each of the three storms, and at each application a 3 L solution containing ~20–25 ppm of the REE tracer was sprayed. Immediately after the onset of rain, we collected the outflow at 5–10 min intervals using 125 mL polypropylene bottles (precleaned with Citrinox).

Water samples were acidified to 1 wt % nitric solution using ultrapure nitric acid (Seastar, Canada) and analyzed for REE concentrations using high-resolution inductively coupled plasma-mass spectrometer (ICP-MS) (Finnigan Element). Samples of the tap water and the original spray solutions were also analyzed for Tm, Yb, and Lu concentrations. The relative standard deviation for the chemical analyses is within 5%.

3. Results

To establish baseline concentrations for our REE tracers, we analyzed the tap water, the fresh snow sampled throughout the season, and a clean snow profile sampled in April. The tap water contained 2.7, 1.5 and <1 parts per trillion (ppt) of Tm, Yb, and Lu, respectively. The average concentration of Tm, Yb, and Lu in fresh snow (10 samples) and the snow profile (26 samples) are all below 1 ppt, with the highest concentrations of 2.2, 2.4 and <1 ppt for Tm, Yb, and Lu, respectively. The concentrations of the spikes in the solutions sprayed onto the snow surface were 24.1 ppm for Tm, 20.9 ppm for Yb, and 19.9 ppm for Lu. Compared to the concentration of the applied

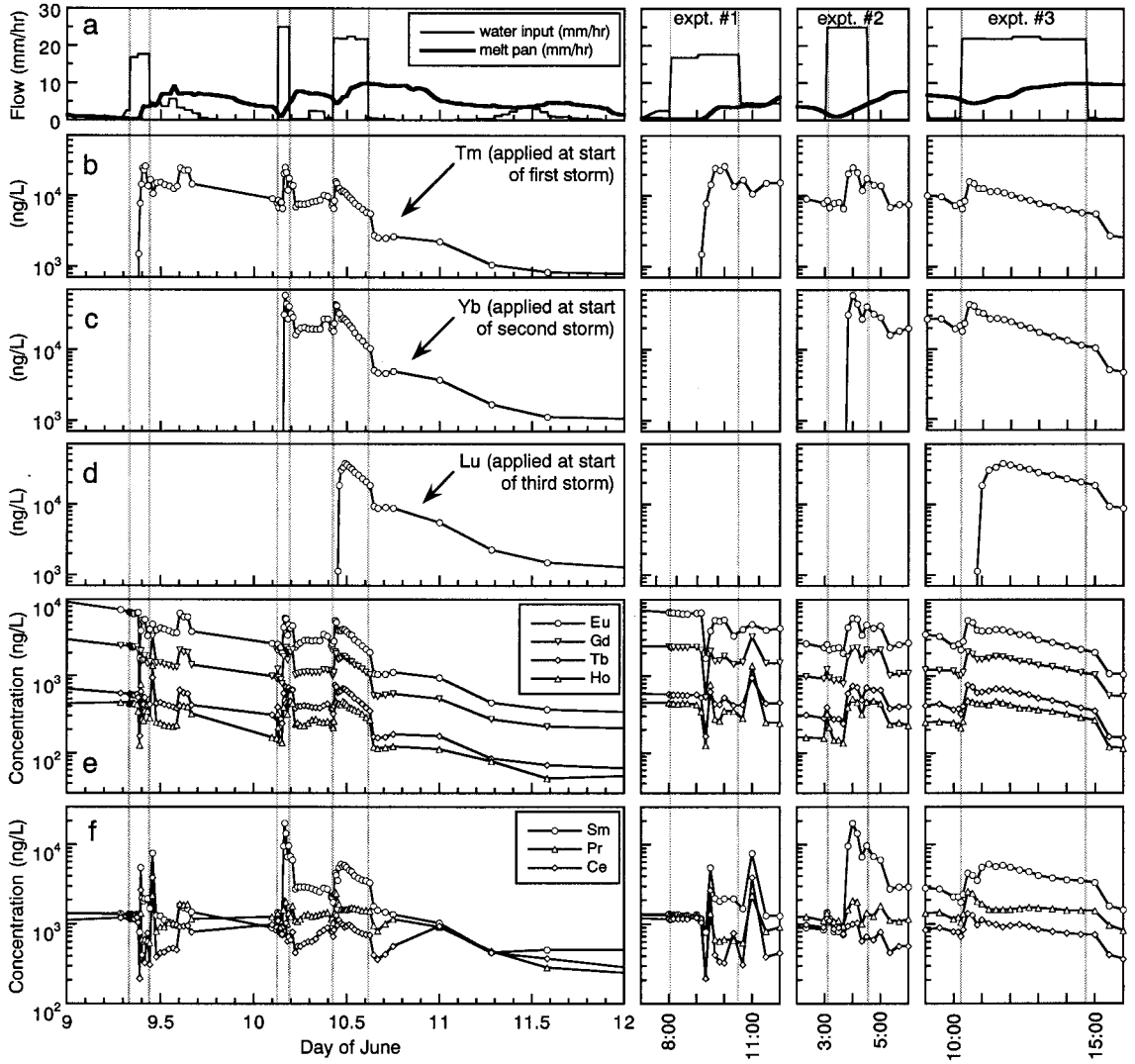

Figure 1. Experimental results from artificial rain-on-snow events. In each row the left-hand panel shows a 3-day time series surrounding the experiments, and the three right-hand panels show details of the three artificial rain-on-snow events. The thin gray lines indicate the beginning and end of each artificial rainstorm. (a) Water input and output fluxes (thin and thick lines, respectively) indicating delayed and damped hydrologic response. (b)–(d) Outflow concentrations of tracers that were applied to the snowpack surface immediately before each of the three artificial rainstorms. Initial arrival of each storm's tracer indicates arrival of rainwater at the bottom of the snowpack. (e) Outflow concentrations of tracers that had been used to tag snowpack layers which melted before the artificial rainstorms [*Taylor et al.*, 2001]. These tracers were translocated (and presumably were dispersed throughout the remaining snowpack) by meltwater. (f) Outflow concentrations of tracers that had been used to tag snowpack layers which were at (Sm) or below (Pr, Ce) the snow surface during the artificial rainstorms. Pr and Ce reflect the behavior of snow in situ within the melting pack. Sm reflects the behavior of snow melting at the snowpack surface, because the snow layer containing Sm was exhumed and melted during our three simulated rainstorms. All the tracer concentrations rose abruptly a short time after the onset of each storm and fell sharply at the end of each storm. The tracer concentrations responded more rapidly in the second and third experiments, when the snowpack was wetter. Note that the tracer concentrations responded strongly to changes in the rainfall flux but not to changes in the outflow flux.

tracer solutions, the baseline of snow and the tap water is at least 7 orders of magnitude lower in all REEs used for the experiments and can be considered essentially as zero.

The results of the rain-on-snow experiments are summarized in Figure 1, which contains both hydrological and chemical measurements as functions of time. The total water input at the snow surface includes artificial rain, natural rainfall, and calculated snowmelt (using the net radiative flux). The three artificial rainstorms are clearly shown in the input flux to the snow surface. Each storm caused the outflow flux to increase but by less than one half as much as the input flux. Furthermore, after the end of a storm, the snowpack continued to drain at a nearly constant rate for many hours (Figure 1a). The total measured discharge (330 mm) during the 3-day experimental period exceeds the total input water (240 mm) by 38%. Snowmelt due to tap water only contributed ~2 mm of dis-

charge, and it is likely that the snowpack was wetter at the end than at the beginning of the experiment. Because the sprayed area was greater than the surface area of the pan, it is possible that some water sprayed outside of the pan drained into it.

The REE tracer concentration time series show four features. First, the time it took for each storm's tracer to reach the bottom decreased with increasing wetness of the snowpack. The experiment with Tm (storm 1) started in a cold morning when the discharge was very low. It took ~70 min for Tm to appear in the outflow (Figure 1b). In storms 2 and 3, which started in increasingly wet conditions, Yb (storm 2) and Lu (storm 3) reached the bottom in ~50 and 40 min, respectively (Figures 1c and 1d).

Second, the tracer concentrations responded sharply, and promptly, to the input water flux (but not the outflow flux); high concentrations were associated with high rainfall fluxes and vice versa. For example, immediately after the onset of storm 3, the concentrations of both Tm and Yb, which had been applied in earlier storms, increased by more than a factor of 2, and shortly after the artificial rain stopped, their concentrations decreased abruptly, again by more than twofold (Figures 1b and 1c). Similar responses were observed in the tracers that marked individual snow layers, including those that had been translocated by meltwater (Figure 1e) and those that marked snow layers that were still in situ (Figure 1f). These concentration changes did not accompany any abrupt change in discharge.

Third, at a constant input flux, the concentrations of all the REE tracers (except Pr) decreased exponentially with time (shown as linear trends on the logarithmic concentration scales shown in Figures 1b–1f). The rate of this decrease was greater at high flow than at low flow.

Fourth, in the third experiment an increase in the surface flux caused the concentration of all of the preexisting tracers to increase at least 20 min before the arrival of Lu at the base of the snowpack (Figures 1b–1f).

4. Discussion

Throughout the winter season many processes in snow may affect the concentrations of natural solutes in snowmelt. For example, snow metamorphism and solute transport redistribute the solutes originally precipitated with fresh snow. These processes are affected by many variables, including air temperature and its daily variations, snow accumulation rate, rain-on-snow events, and the frequency and intensity of melting-freezing cycles. Our artificial rain-on-snow experiments were conducted in well-controlled conditions, so that we can ignore several complicating factors that were either absent or relatively unimportant. The experimental design allows us to make the following assumptions: (1) The tracers that we applied were not present in the snowpack prior to the experiments; (2) The snowpack was fully ripe and isothermal, and the hydrological properties (porosity and permeability) did not change (although this may not be valid because grain growth may occur under high saturation); (3) No freezing occurred within the pack (freezing at the snow surface might have occurred in the morning of June 9 before the first experiment because of radiative cooling, but we believe that no freezing occurred during this experiment and throughout the subsequent rain-on-snow events); and (4) The snowpack had a nearly constant thickness.

Thanks to the relatively well-defined experimental conditions, we can test different flow models and constrain flow mechanisms. In the following sections we begin by estimating the effective water saturation, an important hydrological parameter, using the observed flow velocities and appropriate flow equations. Then we discuss solute transport mechanisms using a solute transport model.

4.1. Effective Saturation of the Snowpack

Colbeck [1972] made the first theoretical treatment of water percolation through homogeneous snow and showed that the volume flux of water, Q, can be approximated as

$$Q = KS^n, \tag{1}$$

where K is a constant, and for a given intrinsic permeability k of a medium,

$$K = \frac{\rho k g}{\mu}, \tag{2}$$

where ρ, g, and μ are the water density, gravitational acceleration and water viscosity, respectively. S in (1) is the effective water saturation defined by *Colbeck* [1972] (Table 1) and n is an empirical exponent. The constitutive flow equation (1) defines, by mass conservation, the following governing equation for one-dimensional water percolation in snow [*Colbeck and Davidson*, 1972; *Hibberd*, 1984],

$$\frac{\partial S}{\partial t^*} + \frac{K}{\phi(1 - S_i)} \frac{\partial S^n}{\partial z^*} = 0, \tag{3}$$

where ϕ is porosity, S_i is the irreducible water content in the snowpack, z^* is the depth into the snowpack, and t^* is time. The water velocity u^* is dependent upon the flow mechanism. For piston flow, in which the irreducible water moves down the hydraulic gradient with the bulk water, u^* is expressed as

$$u^* = \frac{KS^n}{\phi S_w} = \frac{KS^n}{\phi(1 - S_i)(S + \beta)}, \tag{4}$$

where S_w is the fraction of total water volume in pore pace and $\beta = S_i/(1 - S_i)$. If the irreducible water is relatively immobile and only the effective water content has a velocity (preferential flow condition), u^* becomes

$$u^* = \frac{KS^n}{\phi(S_w - S_i)} = \frac{KS^{n-1}}{\phi(1 - S_i)}. \tag{5}$$

From the arrival time of the three tracers the effective water flow velocity can be calculated to be ~1.9 to 3.3 cm min^{-1}. Because of hydraulic dispersion the first appearance of the tracer will occur somewhat earlier than the average water pulse carrying the tracer from the surface. This delay is likely to be ~20 min for the first storm and 10 to 5 min for the second and third storms (Figure 1). This yields water velocities of 1.4 to 2.9 cm min^{-1}. Using 6×10^{-9} m^2 as the intrinsic permeability of the snowpack [*Wankiewicz*, 1978] and $n = 3$ [*Colbeck and Anderson*, 1982; *Wankiewicz*, 1978], we calculate that the effective saturation of the snowpack was within the range of 0.08–0.11 for piston flow (equation (4)) and 0.06–0.09 for preferential flow (equation (5)).

4.2. Relationship Between Water Flux and Tracer Concentration

Covariations of discharge and solute concentration have been observed previously. Most frequently, high discharges are

Table 1. Symbols

Symbol	Meaning	Units	First Used in Equation
α	exchange rate constant	s^{-1}	(6)
β	$S_i/(1 - S_i)$		(4)
C_m	tracer concentration in mobile phase	$\mu g\ L^{-1}$ or $ng\ cm^{-3}$	(6)
C_i	tracer concentration in immobile phase	$\mu g\ L^{-1}$ or $ng\ cm^{-3}$	(6)
d	dynamic dispersivity	cm	(19)
D^*	dispersion coefficient	$cm\ s^{-1}$	(6)
D	dimensionless dispersion coefficient		(9)
g	gravitational acceleration	$cm\ s^{-2}$	(2)
k	intrinsic permeability	cm^2	(2)
K	hydraulic conductivity	$cm\ s^{-1}$	(1)
n	exponent		(1)
ρ	density of water at 0°C	$g\ cm^{-3}$	(2)
Q	specific discharge	$cm\ s^{-1}$ ($mm\ h^{-1}$)	(1)
γ	dimensionless exchange rate constant $\gamma = \alpha Z/K$		(12)
S	effective water saturation $(S_w - S_i)/(1 - S_i)$		(1)
S_i	irreducible water content: irreducible volume of water over pore volume		(3)
S_w	total water content: total water volume over the pore volume		(4)
t^*	time	s	(3)
t	dimensionless time		(8)
u^*	water velocity	$cm\ s^{-1}$	(4)
u	dimensionless water velocity		(9)
μ	viscosity of water at 0°C	$dyn\ s\ cm^{-2}$	(2)
V^*	wave velocity	$cm\ s^{-1}$	(1)
V	dimensionless wave velocity		(1)
z^*	depth	cm	(3)
z	dimensionless depth		(8)
Z	total depth of the snowpack	cm	(8)
ϕ	porosity		(3)

observed to be associated with low solute concentrations in diurnal cycles of melting [e.g., *Bales et al*., 1993; *Davis et al*., 1995; *Williams and Melack*, 1991]. Two explanations have been given for this observation. First, freezing of liquid water running down the snow column at cold temperatures causes reduction of discharge and concentration of the solute [*Colbeck*, 1977; *Colbeck*, 1981; *Davis et al*., 1995; *Williams and Melack*, 1991]. Since no freezing occurred in this experiment, we can ignore this mechanism. Second, decreasing concentrations with increasing discharge have been attributed to preferential flow. The liquid water in snow is viewed to be in different pools or flow paths. These pools are characterized by different flow velocities (e.g., flow fingers versus matrix) and chemical concentrations. Waters in these pools mix with proportions that vary with flow velocity. Usually flow channels that are more permeable will have lower solute concentrations because of efficient flushing. Dye tracer experiments have revealed areas of concentrated dye and flow fingers with clean meltwater [*Harrington et al*., 1996].

Piston flow models cannot explain either the flow-concentration relationship typically observed in diurnal cycles (low concentrations at high flow) or the response we observed in our artificial storm events (increasing concentrations with increasing rainfall rates). *Hibberd* [1984] described a piston flow model for snow, in which water simply reaches the bottom in the sequence it is melted at the surface. If the water having high solute concentrations were assumed to be initially present in the irreducible water, the first wetting front would remove most of the solutes by pushing out the concentrated pore water. With an incorporation of hydraulic dispersion and an assumed constant melt rate, Hibberd obtained a characteristic exponential decrease in the solute concentrations of discharge, which successfully explained the generation of ionic pause. However, the observed association between the solute concentration and flow rate cannot be produced by the model because it does not acknowledge the existence of multiple pools of water having different solute concentrations and flow rates.

The simplest treatment of preferential flow is to assume that the microscopic pore water velocity has a bimodal distribution, which partitions the liquid water into mobile and immobile phases. Solutes in the mobile phase are carried by percolating water, but those in the immobile phase can be transported only by exchanging with the mobile phase. Because of continuous flushing the mobile phase typically has lower solute concentrations than the immobile phase [*Harrington et al*., 1996]. In addition, the bulk snow to be melted at the surface is usually cleaner than either the mobile or immobile fraction of the liquid water because the ice has been purified of most contaminants during snow metamorphism [e.g., *Cragin et al*., 1996]. If the rate of exchange between the mobile and immobile phases is more or less constant, high flows (high melt rate) would result in relatively low solute concentrations because of dilution.

Harrington and Bales [1998] developed a physically based model to describe solute concentrations in snowmelt. The model considered metamorphic processes involving freezing and melting, as well as the dual-velocity nature of the snowpack. The solute behavior of the mobile phase is described by an advection-dispersion equation, and the mobile and immobile waters exchange is described with a fixed rate constant. This model can produce decreases in solute concentrations with the rising limb of diel wetting fronts but does not explain the concentration increases with increasing water flux seen in our data [also see *Berg*, 1991]. We propose a modification of

the model that may explain our observations without fundamentally changing the flow mechanism. In this model we assume that the exchange rate constant is not fixed but instead increases with flow velocity (or the effective water content). This model is described in sections 4.3. and 4.4.

4.3. A Solute Transport Model

Our solute transport equations are similar to those developed by *Harrington and Bales* [1998]. Symbols used in the derivation are summarized in Table 1. The governing equation for the mobile phase is

$$S\frac{\partial C_m}{\partial t^*}+\frac{\partial(u^*SC_m)}{\partial z^*}=\frac{\partial}{\partial z^*}\left(SD^*\frac{\partial C_m}{\partial z^*}\right)+\frac{\alpha}{\phi(1-S_i)}(C_i-C_m) \tag{6}$$

and for the immobile phase is

$$\frac{\partial C_i}{\partial t^*}=\frac{\alpha}{\beta\phi(1-S_i)}(C_m-C_i), \tag{7}$$

where C_m and C_i are the tracer concentrations in the mobile and immobile water fractions, respectively, α is the rate constant for exchange between mobile and immobile phases, and D^* is the dispersion coefficient. It is more convenient to discuss the calculations with dimensionless variables and constants. The variables S, C_m, and C_i are already dimensionless, and following *Hibberd* [1984], we nondimensionalize the other variables using the following definitions:

$$z=\frac{z^*}{Z},\qquad t=\frac{Kt^*}{\phi(1-S_i)Z}, \tag{8}$$

where Z is the total depth of the snowpack and z and t are nondimensional depth and time. Other nondimensional variables have the form

$$u=\frac{\phi(1-S_i)u^*}{K},\qquad D=\frac{\phi(1-S_i)D^*}{KZ}. \tag{9}$$

Introducing nondimensional variables, (1), (5), (6), and (7) become

$$\frac{\partial S}{\partial t}+\frac{\partial S^n}{\partial z}=0 \tag{10}$$

$$u=S^{n-1} \tag{11}$$

$$S\frac{\partial C_m}{\partial t}+\frac{\partial(uSC_m)}{\partial z}=\frac{\partial}{\partial z}\left(SD\frac{\partial C_m}{\partial z}\right)+\gamma(C_i-C_m) \tag{12}$$

$$\frac{\partial C_i}{\partial t}=\frac{\gamma}{\beta}(C_m-C_i), \tag{13}$$

where $\gamma=\alpha Z/K$ is the dimensionless form of the mobile-immobile exchange rate constant.

To simplify the calculations, we assume that a simple sequence of changes in water flux occurs at the snow surface. The goal is to examine the behavior of tracer concentrations when the surface flux changes, stepwise, from high to low or from low to high. We parameterize γ, the dimensionless rate constant for mobile-immobile exchange, in two different ways and compare the results. In the first case, γ is assumed to be constant, and in the second, γ is an exponential function of S. Initially, the snowpack is assumed to be dry ($S=0$) and the tracer applied to the surface is contained in the immobile water in the top 5% of the pack.

For the tracer concentration in the mobile phase the snow surface has a no-flux boundary condition,

$$uC_m-D\frac{\partial C_m}{\partial z}=0, \tag{14}$$

and at the bottom we use free-draining condition $D=0$ so that

$$\frac{\partial C_m}{\partial t}+u\frac{\partial C_m}{\partial z}=\frac{\gamma}{S}(C_i-C_m). \tag{15}$$

When there is a discontinuity of water content (wave front) in the snowpack, the position of the wave front is determined by the wave velocity, V^*,

$$V^*=\frac{K}{\phi(1-S_i)}\frac{S_+^n-S_-^n}{S_+-S_-}, \tag{16}$$

where the subscripts plus and minus represent values directly behind and preceding the wave front [*Hibberd*, 1984]. The dimensionless wave velocity is

$$V=\frac{\phi(1-S_i)V^*}{K}=\frac{S_+^n-S_-^n}{S_+-S_-}. \tag{17}$$

The chemical composition at either side of the wave front satisfies the mass conservation relation,

$$V[S_+C_{m+}+\beta C_{i+}-S_-C_{m-}-\beta C_{i-}]=S_+^nC_{m+}-S_-^nC_{m-}-S_+D_+\frac{\partial C_{m+}}{\partial z}+S_-D_-\frac{\partial C_{m-}}{\partial z}. \tag{18}$$

The value of D^* is assumed to be dependent upon water velocity such that

$$D^*=du^*, \tag{19a}$$

and therefore

$$D=\frac{d}{Z}u, \tag{19b}$$

where d is the dynamic dispersivity [*Hibberd*, 1984] (we ignore molecular diffusion). In all of the following calculations we used 0.05 for d/Z. Equations (12) and (13) are solved numerically, with the boundary and initial conditions described above.

4.4. Results of Model Calculations

4.4.1. Concentration change when water flux increases at the surface. Figure 2 compares how the tracer concentration changes upon a sudden increase in the water flux at the surface for constant and variable γ, respectively. The dimensionless water velocity at the upper and lower boundary as a function of time is illustrated in Figures 2a and 2c. At the surface the water content increases from 0 to 0.06 at $t=0$ and again to 0.1 at $t=694$. Because the snow column is dry initially, there is no outflow until $t=275$ when the water introduced to the surface has traveled through the column. When the surface flux increases again at $t=694$, the response of discharge occurs at $t=746$, much more rapidly than for the initial wetting. This is because the wave propagation is faster through a wet snow-

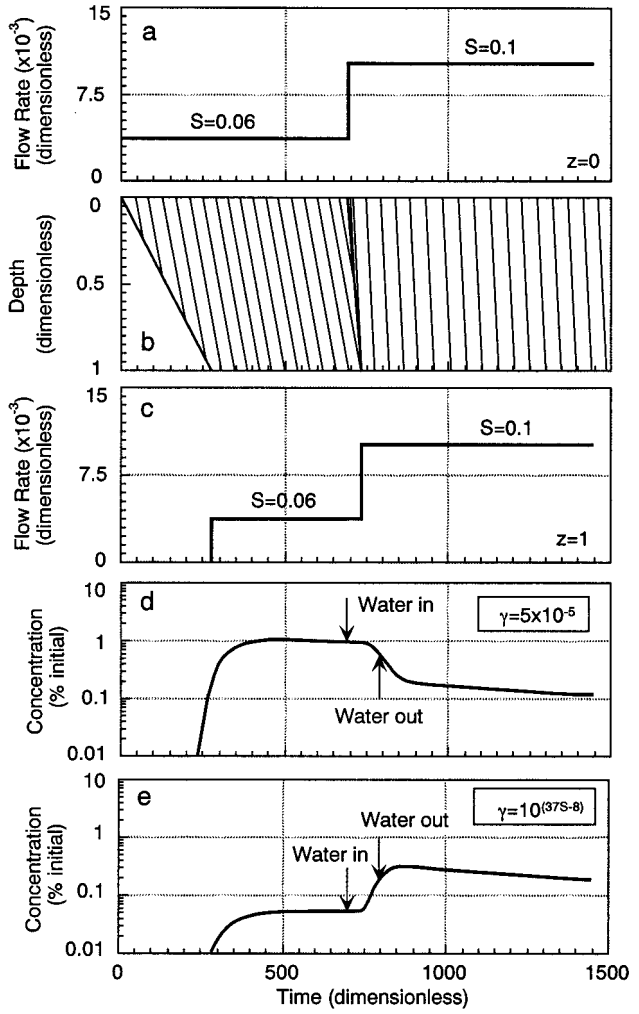

Figure 2. Modeling results for an increase in water flux. (a) Water flux at the surface of the snowpack. Initially, the pack is dry and discharge is zero. At $t = 0$ the effective water content S at the surface is increased to 0.06 and then increased again at $t = 694$ to 0.1. (b) Characteristic lines, showing shock waves (in thick lines) from $t = 0$ to 275 and from $t = 694$ to 746. (c) Water flux at the bottom of the snowpack. (d) Tracer concentrations with a constant exchange rate coefficient ($\gamma = 5 \times 10^{-5}$). (e) Tracer concentrations assuming that the exchange rate coefficient varies exponentially with water content ($\gamma = 10^{(37S-8)}$). The arrows show the time of the disturbance ("Water in," $t = 694$) and the time when water introduced at $t = 694$ reaches the bottom ("Water out"). Note in Figure 2e the concentration increases after the flux is increased. At a constant flux (e.g., $t > 1000$), the concentration decreases exponentially with time. Other parameters are $S_i = 0.05$, $d/Z = 0.05$, and $n = 3$.

pack than a dry one. The characteristic lines for the solution of (1) are shown in Figure 2b, in which the positions of the wave fronts are shown as thick lines.

We found that in order for low tracer concentrations to accompany low water fluxes, γ has to increase exponentially with the water content S, as follows:

$$\gamma = 10^{(37S-8)}. \tag{20}$$

Equation (20) predicts a fivefold change in the exchange coefficient γ, as S changes from 0.06 to 0.1. This parameterization is chosen to best fit the observation of Lu (see Figure 4).

The modeled time series of solute concentrations are shown in Figure 2d for constant $\gamma = 5 \times 10^{-5}$ and Figure 2e for γ varying according to (20). With the exchange rate coefficient between mobile and immobile phases held constant the solute concentration decreases with increasing water flux at the snow surface (Figure 2d). When the exchange rate constant increases exponentially with S, we produce a positive relationship between the solute concentration and water flux (Figure 2e). This result compares well with the observed variations of Tm and Yb during the second and third experimental storms, when the water flux increased suddenly at the surface.

We indicated in Figures 2d and 2e the time at which water flux increases at the surface ($t = 694$). The water introduced to the pack at this moment comes out ~100 time units later, which is also marked in the diagrams. This time ($t = 794$) lags the time when discharge increased at the bottom ($t = 745$) because the water velocity is less than the kinematic wave velocity. Note that in Figures 2d and 2e the concentration change begins shortly before the water reaches the bottom as a result of dispersion.

It is evident from Figures 2d and 2e that the chemical response of the outflow to a hydrological change at the surface does not occur until the water introduced at the time of the perturbation travels to the bottom (or slightly before that, owing to dispersion). In our experiments the tracers are concentrated in the immobile phase at or near the surface. When the water flux changes at the surface, it changes the mixing of the immobile water to the mobile water and thus the chemical composition of the latter. In the calculation with a constant γ the increase in water flux would cause a decrease in tracer concentration of the mobile water because the same amount of immobile water is mixed into a greater amount of clean water. If, on the other hand, the exchange rate constant increased with water flux, the tracer concentration of the mobile water would depend on two competing factors: the degree of dilution by a greater flux of clean water and increased incorporation of immobile water with high solute concentrations. When the latter outweighs the former, the concentration of the mobile phase increases as shown by our calculation using the parameterization of (20) (Figure 2e).

Figures 2d and 2e also show that when the flux at the snow surface is constant, e.g., at $t > 1000$, the solute concentration decreases exponentially. This agrees well with our observations (Figure 1). During the third storm, which lasted 4.5 hours, all three tracer concentrations decreased exponentially with time. This suggests that there is a reservoir of tracers that is being mixed into the mobile water and its own concentration decreases exponentially with time. Our model successfully describes this physical process.

4.4.2. Concentration change when water flux decreases at the surface. Figure 3 compares how the tracer concentration changes upon a sudden decrease in the water flux at the surface for constant and variable γ, respectively. The arrangement of the diagrams within Figure 3 is the same as that in Figure 2. At the surface the effective water content increases from 0 to 0.1 at $t = 0$ and then decreases to 0.06 at $t = 500$. The hydraulic response of outflow to the initial wetting at $t = 0$ occurs at $t = 100$ (Figure 3b), which is quicker than in the previous calculation (Figure 2b) because of the higher water velocity assumed here. When the flux at the surface suddenly decreases,

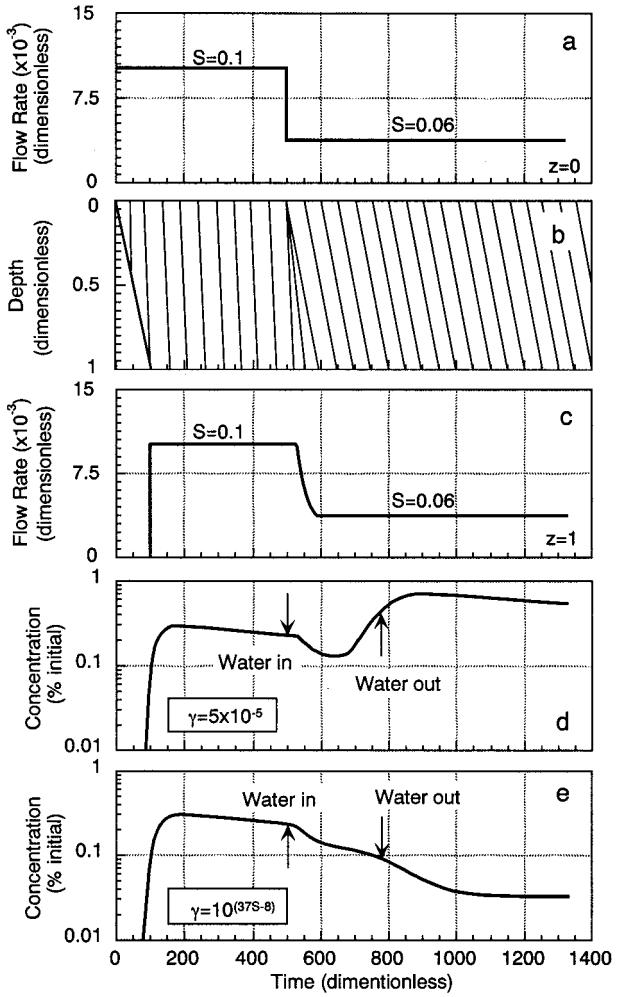

Figure 3. Modeling results for a decrease in water flux. (a) Water flux at the surface of the snowpack. Initially, the pack is dry and discharge is zero. At $t = 0$, S at the surface increased to 0.1 and then decreased to 0.06 at $t = 500$. (b) Characteristic lines, showing the shock wave from $t = 0$ to 100 and expansion wave from $t = 533$ to 580. (c) Water flux at the bottom of the snowpack. (d) Tracer concentrations with a constant exchange rate coefficient ($\gamma = 5 \times 10^{-5}$) between mobile and immobile phases. (e) Tracer concentrations assuming that the exchange rate coefficient varies exponentially with water content ($\gamma = 10^{(37S-8)}$). The arrows show the time of the disturbance ("Water in," $t = 500$) and the time when water introduced at $t = 500$ reaches the bottom ("Water out"). Note in Figure 3e the concentration decreases with decreasing flux. At a constant flux, the concentration decreases exponentially with time, and the slope of the decrease is steeper for high flow than for low flow. Other parameters are $S_i = 0.05$, $d/Z = 0.05$ and $n = 3$.

the flux of outflow decreases continuously to the new input level (Figure 3c).

As predicted, the chemical response of the discharge to the reduction of input flux is opposite, depending on whether γ is held constant (in which case solute concentrations decrease at high flow) or γ increases exponentially with S (in which case solute concentrations increase at high flow). The calculation shown in Figure 3e also produces the correct slope of the curve at a constant flow rate. For example, the slope for the time period $200 < t < 500$ (high flow) is greater than the slope at $t > 1000$. A shallower slope indicates a relatively smaller pool of immobile water participating in the exchange with mobile water. This is expressed in the model by reducing the value of γ when the flow rate decreases.

In both Figures 3d and 3e the solute concentration decreases rapidly in the outflow during the time period when the water content at the bottom of the pack decreases from 0.1 to 0.06. This happens because the solute is transported from the surface to the bottom. The chemical flux of this transport is determined by the rate of advection (or the water velocity). When the flux at the surface decreases, it quickly propagates through the entire column, causing a reduction of water velocity at all depths. The chemical transport slows down accordingly, and the concentration of the outflow decreases. This decrease continues until the new chemical condition at the surface propagates to the bottom (or slightly before that because of dispersion), which is indicated by the "Water out" arrows in the diagrams.

The concentration profile shown in Figure 3e generally resembles that of Lu in the third artificial rain-on-snow experiment. In Figure 4 we present a comparison between the observed and calculated Lu concentrations on a dimensional timescale. To make this calculation, we assumed that the total amount Lu applied (60 mg) was evenly distributed in the immobile phase of the upper 5% of the pack (the uppermost grid in the numerical calculation). At the beginning of the experiment (June 10, 10:10 A.M. PST) the effective water content at the surface increased to 0.1 and then 4.5 hours later decreased to 0.025 (June 10, 2:40 P.M. PST). The model qualitatively captures the main features of Lu behavior in the outflow.

4.5. Rate Constant for the Exchange Between Mobile and Immobile Water Fractions

The parameterization of (20) was chosen for the model because it produces model behavior similar to our experimen-

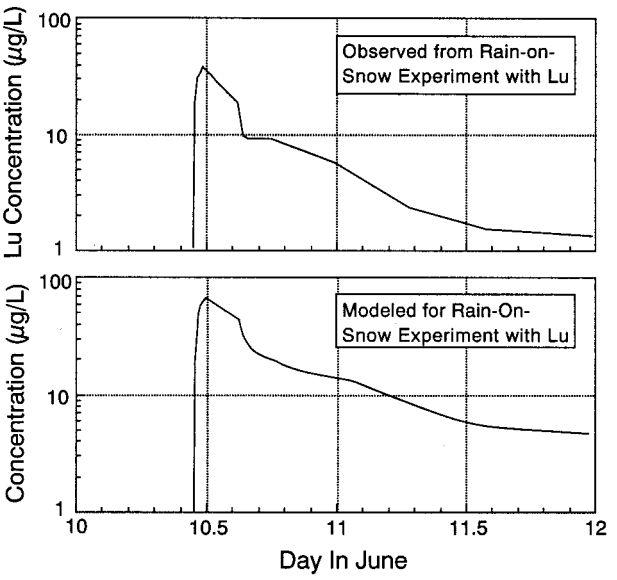

Figure 4. Comparison of the modeled with the observed Lu concentrations as a function of dimensional time. To make the calculation, we assumed that S at the surface increased from 0 to 0.1 at the beginning of storm 3 and decreased suddenly to 0.025 after 4.5 hours. Other parameters are the same as the calculation of the curve in Figure 3e. The model captures the main features of the observation.

tal results. In particular, it generates chemical variations at the outflow that are positively associated with the input flux. As discussed previously, the association of low concentration with high water flux may result from the competing effects of (1) greater input of clean water and (2) greater incorporation of immobile water into the mobile channels. Figure 5 illustrates a few possible scenarios of this competition, corresponding to several different functional relationships between γ and S. Figure 5 indicates that it is possible to have a negative concentration-flow rate relationship even though γ increases with the flow rate (or S). In this case, illustrated by curve b, the effect of dilution outweighs the effect of exchange between mobile and immobile water.

The physical mechanism behind the parameterization of the exchange rate constant needs further exploration. It is plausible that high flow may increase mixing between the mobile and immobile phases, and it may also cause the immobile phase to become mobile. The immobile water is often viewed as water in dead-end pores, thin liquid films around solid particles, and immobile intra-aggregate water or isolated regions associated with unsaturated conditions [*Kutílek and Nielsen*, 1994]. All of these types of immobile water would become more connected with the mobile water when the effective saturation increases. Imagine, for example, that the effective water saturation is sufficiently low that mobile water does not form a continuous film along a flow channel. For the part of the channel that is not in contact with the mobile water, the dead-end pores and the thin liquid films around the solid particles cannot reach the mobile water mechanically, and molecular diffusion would be the only mechanism for their exchange with the mobile phase. When the effective water saturation increases, more of each flow channel will be lined with mobile water. A number of things may result: (1) More dead-end pores may become directly connected with the mobile water, (2) thin liquid films that were immobile may now join the mobile phase, and (3) isolated relatively dry regions in the media may shrink. All these processes underlie the empirical parameterization of the mobile-immobile exchange rate constant as a function of the effective water saturation.

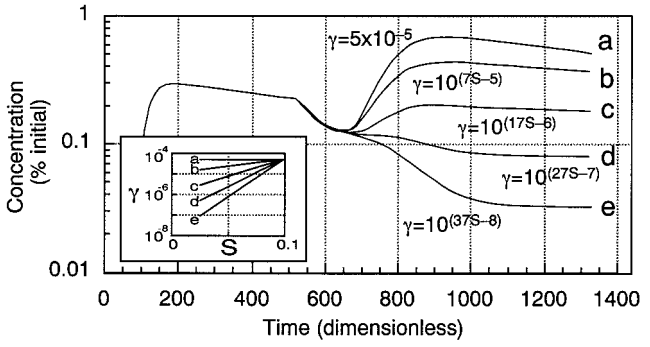

Figure 5. Comparison of the concentration-flow rate relationship for different parameterizations of γ, other parameters being identical to the calculation shown in Figure 3e. The intercepted diagram illustrates the functional dependency of γ on S. In all cases except for curve a, γ decreases exponentially with S. Curve b indicates that a negative concentration-flow relationship can be obtained even though the exchange rate constant decreases with the decreasing flow rate. In this case, less dilution with a low water flux outweighs the reduced contribution of immobile water to the mobile phase.

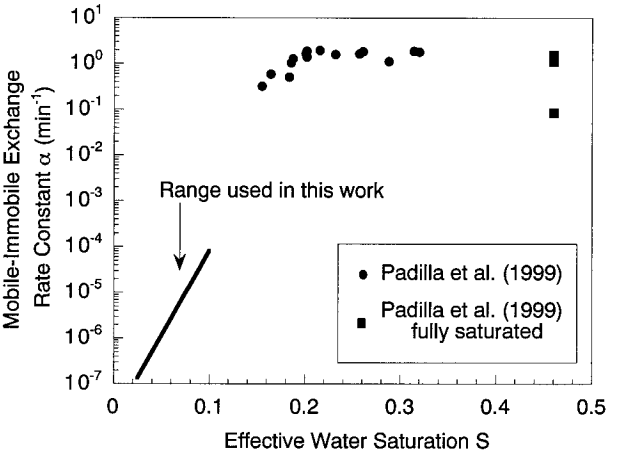

Figure 6. Comparison of the rate constant for mobile-immobile exchange, α, between our parameterization of snow and those of sand by *Padilla et al.* [1999]. The value of α levels off, approaching a constant, at $S \approx 0.2$.

Given the above description of the immobile phase and the mechanisms of its exchange with the mobile phase, it is required that the empirical constant γ (or its dimensional counterpart α) should not increase infinitely with the water content. The value of α should approach a constant value as the medium approaches saturation. In fact, a constant α should be reached when there is enough mobile water to form a continuous film lining the flow channels, which is likely to occur well below saturation. The dependency of α on water content has been observed both in sand column experiments [*Padilla et al.*, 1999] and in the field [e.g., *Pang and Close*, 1999]. Figure 6 compares the α values of our experiments with those from *Padilla et al.* [1999], who showed that α increases exponentially with S until ~20% of saturation ($S \approx 0.2$).

Our model did not independently consider the fact that the volume of the immobile phase may decrease as the effective water saturation increases. Strictly speaking, once the immobile water becomes mobile, it should be described with advective-dispersive equations, rather than with mobile-immobile water exchange. This requires S_i to be parameterized as a function of S. In snow it is difficult to measure S_i and even more difficult to study its functional relationship with S. Our experimental design cannot provide any basis for parameterizing a relationship between S_i and S. We therefore assume that this mechanism has effects that are similar to increasing the rate of exchange between mobile and immobile phases.

As mentioned earlier, several previous investigations have observed tracer concentrations that decrease at high flow, rather than increase, as we observed in our experiments. This may have occurred for two reasons. (1) The function $\gamma = f(S)$ (or its dimensional counterpart $\alpha = f(S)$) may not have been as steep as the one required by our data, and therefore the effect of dilution would dominate over the increase in mobile-immobile exchange. Curve b in Figure 5 illustrates this possibility. (2) The snowpacks previously studied may have been wetter than the snowpack in our experiments. Under this condition, α may have been high enough that it was insensitive to water content. However, this is unlikely given the large flux of water we introduced into the snowpack. It remains an open question what determines the functional relationship between α and S and how it varies from one snowpack to another.

4.6. Model Limitations and Implications

To summarize the discussions above, the model is successful in two respects: (1) It reproduces the observed positive relationship between the solute concentration in the outflow and the water flux at the snow surface. (2) When the input flux at the surface is constant, the solute concentration of the outflow decreases exponentially. The rate of this decrease is greater at high flow than at low flow. The model, however, does not reproduce two aspects of our experimental observations. First, the observed outflow water mass flux responds much less to changes in the input flux than the model does. Second, the model cannot reproduce the results of the third experiment, in which the arrival of Lu significantly lagged behind the chemical response of Tm and Yb that had been applied earlier.

In all three experiments a sudden change in the input water flux was converted into a gradual change in the discharge. Furthermore, the peak discharge was strongly damped, never reaching half of the input flux (Figure 1). Obviously, the entire pack did not have the same flow velocity, as assumed in the model; instead, water sprayed at the surface reached the bottom over a long time interval, making the outflow response more gradual than the input. Some flow channels were probably so slow that they effectively stored water during the artificial rain and slowly drained it out many hours after the storm. This hydrological phenomenon is not surprising. It is striking, however, that the chemical response of the discharge was almost entirely dominated by the fast flow. This inference is supported by two pieces of evidence. First, the tracer concentration quickly responded to the input flux rather than to the discharge. At the end of the third experiment, for instance, the concentrations of all three tracers dropped by about a factor of 2 immediately after the end of the storm, while the discharge stayed constant. This suggests that the portion of water that flows quickly carry most of the solutes in the total flow. In other words, the concentration of the outflow is largely determined by the rate of solute delivery by the fast flow paths, over the timescale of our observation.

The second piece of evidence comes from our model parameterization. We used $S = 0.1$ as the effective water content in the snowpack during the third storm. This value is calculated from the water velocity inferred from the arrival time of Lu. The water flux corresponding to this value (for this snowpack) is $\sim$100 mm h^{-1} (equation 1), which is 3–4 times greater than the input flux of the storm and 8 times greater than the discharge (Figure 1). Assuming all the active flow channels have this effective saturation and flow rate, they must represent roughly 10% of the total cross section area of the pack. Considering that slow flow paths also contribute to the total outflow, the value may be significantly lower than 10%. To model the observed Lu concentration curve (Figure 4) after the storm, we needed to reduce the surface flux from $S = 0.1$ to $S = 0.025$. The value $S = 0.025$ corresponds to a water flux of about 2 mm h^{-1}, which is much lower than the discharge level (10 mm h^{-1}) that was sustained many hours after the artificial rain. This further indicates that although some slow flow paths are hydrologically important to the outflow flux, they appear to be less significant for solute transport than the fast flow channels.

Is the immobile water really immobile? It is assumed so in our model, but our experimental data suggest that this may not be entirely the case. This conclusion comes from the fact that in the third experiment all of the other REE tracers increased in the discharge measurably before the arrival of Lu. When a sudden increase in water flux occurs at the surface, this disturbance propagates down the column faster than the water itself. This means that the flow velocity or the effective water content at a given depth would increase before the water introduced at the time of disturbance reaches that depth. In the portion of the pack where the water content has increased, faster exchange between mobile and immobile water will occur. Therefore the discharge chemistry may be affected before the water of the disturbance itself appears at the bottom. This is consistent with the fact that concentrations of all tracers applied before the artificial storms increased before Lu arrived. Some of these tracers, such as Ce, were present in the immobile phase near the bottom (35 cm from the base) of the snowpack. The timing of Tm and Yb responses is not measurably different from the prestorm tracers. This can only happen if the immobile water well below the surface is concentrated in Tm and Yb, which requires the immobile water to move downward before the third storm. An approximate calculation suggests that for Tm and Yb concentrations to increase in the outflow 20 min before the arrival of Lu, the "immobile" water must have moved down the snowpack by $\sim$60 cm, almost halfway through the total depth of 130 cm.

To characterize the movement of "immobile" water as well as "mobile" water, a dual-permeability model is required. This model has been used to describe a structured soil [*Gerke and van Genuchten*, 1993] in which interaggregate pores and intraaggregate pores are considered as two interconnected permeability systems. However, dual-permeability models require many parameters, some of which cannot be easily measured experimentally. The question is then whether the mobile-immobile model is sufficiently accurate to describe solute transport processes in seasonal snowpacks. We believe that our model has effectively explained the most important features of our experimental observations. To extend this model to a greater spatial and temporal scale, it needs to be tested with more experiments under diverse hydrological conditions and snowpack characteristics.

5. Conclusion and Significance

We studied solute transport mechanisms in snow using REE tracers and artificial rain-on-snow events. Unlike previous studies, we observed that tracer concentrations in discharge are positively correlated with the input water flux. This observation cannot be explained by a homogeneous advective-dispersive model, because it does not produce any concentration dependency on water flux. A dual-velocity model, in which water is partitioned into mobile and immobile fractions, is required. In such a model, mobile water is described with advective-dispersive equations, and immobile water exchanges with the mobile water with the first-order kinetics. However, to produce the positive correlation between the solute concentration and water flux, the exchange rate constant has to increase sufficiently steeply with the effective water content. This has not been previously described for snow.

We conclude that how mobile and immobile water interact with each other is an important aspect of solute transport processes because it determines how solutes (contained in the immobile phase) in snow and soil media are released to the groundwater and streams under different hydrological conditions. The parameterization of the mobile-immobile water exchange rate constant may be affected by the nature of the

medium (grain size, heterogeneity, etc.) and the degree of saturation.

Our experimental data show that the tracer concentrations in the discharge are predominately controlled by the fast flow paths. This results in the prompt chemical response of the outflow to the input flux and its relative insensitivity to the discharge. This brings an important question: Is the spatially averaged infiltration rate sufficient to describe the solute transport behavior? Our experimental results indicate that it is not. This work suggests that solute transport behavior at the microscopic pore scale depends upon the velocity distribution in that scale. This velocity distribution is further dependent upon the homogeneity and the hydrological conditions (e.g., wetness) of the medium. Understanding the velocity distribution for a given medium under a given hydrological condition remains a significant challenge for unsaturated zone hydrochemists.

Acknowledgments. This research was supported by a number of NSF grants, including ATM-9628759 and EAR-9903281 to X. Feng, EAR-9357931 to J. W. Kirchner, and EAR-9796293 to C. E. Renshaw. The Central Sierra Snow Laboratory is owned by the U.S. Forest Service and operated by the University of California, Berkeley. Discussions with W. Yang were particularly helpful, and the manuscript has been improved by the comments of R. Harrington and M. Schneebeli.

References

Bales, R. C., R. E. Davis, and D. A. Stanley, Ion elution through shallow homogeneous snow, *Water Resour. Res*., *25*, 1869–1878, 1989.

Bales, R. C., R. E. Davis, and M. W. Williams, Tracer release in melting snow: Diurnal and seasonal patterns, *Hydrol. Processes*, *7*, 389–401, 1993.

Berg, N. H., Ion elution and release sequence from deep snowpacks in the central Sierra Nevada, California, *Water Air Soil Pollut*., *61*, 139–168, 1991.

Cadle, S. H., J. M. Dasch, and R. V. Kopple, Composition of snowmelt and runoff in northern Michigan, *Atmos. Environ*., *21*, 295–299, 1987.

Colbeck, S. C., A theory of water percolation in snow, *J. Glaciol*., *11*(63), 369–385, 1972.

Colbeck, S. C., Tracer movement through snow, *IAHS AISH Publ*., 255–262, 1977.

Colbeck, S. C., A stimulation of the enrichment of atmospheric pollutants in snow cover runoff, *Water Resour. Res*., *17*, 1383–1388, 1981.

Colbeck, S. C., and E. A. Anderson, The permeability of a melting snow cover, *Water Resour. Res*., *18*, 904–908, 1982.

Colbeck, S. C., and G. Davidson, Water percolation through homogeneous snow, in *The Role of Snow and Ice in Hydrology*: *Proceedings of the Banff Symposium*, pp. 242–257, UNESCO, Paris, 1972.

Cragin, J. H., A. D. Hewitt, and S. C. Colbeck, Grain-scale mechanisms influencing the elution of ions from snow, *Atmos. Environ*., *30*, 119–127, 1996.

Davis, R. E., Links between snowpack chemistry and snowpack physics, in *Processes of Chemical Change in Snowpacks*, *NATO ASI Ser*., *Ser. G*, edited by T. D. Davis, H. G. Jones, and M. Tranter, pp. 115–138, 1991.

Davis, R. E., C. E. Petersen, and R. C. Bales, Ion flux through a shallow snowpack: Effects of initial conditions and melt sequences, in *Biogeochemistry of Seasonally Snow-Covered Catchments*, *IAHS-AISH Publ*. 228, edited by K. A. Tonnessen, M. W. Williams, and M. Tranter, pp. 115–126, Int. Assoc. of Hydrol. Sci., Gentbrugge, Belgium, 1995.

Dickson, W., Properties of acidified waters, in *Proceedings of the International Conference on Ecological Impact of Acid Precipitation*, edited by D. Drablos and A. Tollan, pp. 75–83, SNSF Proj., Johs. Grefslie Trykkeri ALS, Mysen, Norway, 1980.

Galloway, J. N., G. R. Hendrey, C. L. Schofield, N. E. Peters, and A. H. Johannes, Processes and causes of lake acidification during spring snowmelt in the west-central Adirondack Mountains, New York, *Can. J. Fish. Aquat. Sci*., *44*, 1595–1602, 1987.

Gerke, H. H., and M. T. van Genuchten, A dual-porosity model for simulating the preferential movement of water and solutes in structured porous media, *Water Resour. Res*., *29*, 305–319, 1993.

Harrington, R., and R. C. Bales, Modeling ionic solute transport in melting snow, *Water Resour. Res*., *34*, 1727–1736, 1998.

Harrington, R., R. C. Bales, and P. Wagnon, Variability of meltwater and solute fluxes from homogeneous melting snow at the laboratory scale, *Hydrol. Processes*, *10*, 945–953, 1996.

Hibberd, S., A model for pollutant concentrations during snow-melt, *J. Glaciol*., *30*(104), 58–65, 1984.

Johannessen, M., and A. Henriksen, Chemistry of snow meltwater: Changes in concentration during melting, *Water Resour. Res*., *14*, 615–619, 1978.

Kutílek, M., and D. Nielsen, *Soil Hydrology*, Catena Verlag, Reiskirchen, Germany, 1994.

Lee, J. H., and R. H. Byrne, Examination of comparative rare earth element complexation behaviour using linear free energy relationships, *Geochim. Cosmochim. Acta*, *56*, 1127–1137, 1992.

Lee, J. H., and R. H. Byrne, Complexation of trivalent rare earth elements (Ce, Eu, Gd, Tb, Yb) by carbonate ions, *Geochim. Cosmochim. Acta*, *57*, 295–302, 1993.

Padilla, I. Y., T.-C. J. Yeh, and M. H. Conklin, The effect of water content on solute transport in unsaturated porous media, *Water Resour. Res*., *35*, 3303–3313, 1999.

Pang, L., and M. Close, Field-scale physical non-equilibrium transport in an alluvial gravel aquifer, *J. Contam. Hydrol*., *38*, 447–464, 1999.

Skartveit, A., and K. T. Gjessing, Chemical budgets and chemical quality of snow and runoff during spring snowmelt, *Nord. Hydrol*., *10*, 141–154, 1979.

Taylor, S., X. Feng, J. W. Kirchner, R. Osterhuber, B. Klaue, and C. E. Renshaw, Isotopic evolution of a seasonal snowpack and its melt, *Water Resour. Res*., *37*, 759–769, 2001.

Tsiouris, S., C. E. Vincent, T. D. Davies, and P. Brimblecombe, The elution of ions through field and laboratory snowpacks, *Ann. Glaciol*., *7*, 196–201, 1985.

Wankiewicz, A., A review of water movement in snow, in *Modeling of Snow Runoff*, edited by S. C. Colbeck and M. Ray, pp. 222–252, U.S. Army Cold Reg. Res. and Eng. Lab., Hanover, N. H., 1978.

Williams, M. W., and J. M. Melack, Solute chemistry of snowmelt and runoff in an alpine basin, Sierra Nevada, *Water Resour. Res*., *27*, 1575–1588, 1991.

X. Feng and C. Renshaw, Department of Earth Sciences, Dartmouth College, Hanover, NH 03755. (xiahong.feng@dartmouth.edu; carl.renshaw@dartmouth.edu)

J. W. Kirchner, Department of Geology and Geophysics, University of California, Berkeley, CA 94720. (kirchner@seismo.berkeley.edu)

B. Klaue, Department of Geological Sciences, University of Michigan, Ann Arbor, MI 48109. (bklaue@umich.edu)

R. S. Osterhuber, Central Sierra Snow Laboratory, Box 810, Soda Springs, CA 95728. (randall@sierra.net)

S. Taylor, U.S. Army Cold Regions Research and Engineering Laboratory, 72 Lyme Road, Hanover, NH 03755-1290. (staylor@crrel.usace.army.mil)

(Received April 7, 2000; revised November 8, 2000;
accepted November 16, 2000.)